*J. metamorphic Geol.*, 1997, **15,** 777–791

# Ductile-brittle transition in pre-Alpine amphibolite facies mylonites during evolution from water-present to water-deficient conditions (Mont Mary nappe, Italian Western Alps)

G. PENNACCHIONI[1] AND B. CESARE[2]
[1]*Dipartimento di Geologia, Palaeontologia e Geofisica, Universita di Padova, Via Giotto 1, I-35137 Padova, Italy (email:pengio@dmp.unipd.it)*
[2]*Dipartimento di Mineralogia e Petrologia, Universita di Padova, C.so Garibaldi 37, I-35137 Padova, Italy*

**ABSTRACT** In the Austroalpine Mont Mary nappe (Italian Western Alps) discrete zones of mylonites–ultramylonites developed from coarse-grained, upper amphibolite facies metapelites of pre-Alpine age. The syn–mylonitic mineral assemblage is quartz–biotite–muscovite–plagioclase–garnet–sillimanite–ilmenite–graphite, and formed via the model hydration reaction:

$$Grt_1 + Kfs + H_2O = Bt_2 + Ilm_2 + Qtz + Ms \pm Sil.$$

Grain-size reduction of about three orders of magnitude was accompanied by extensive recrystallization of all minerals except sillimanite, and by compositional changes of garnet and biotite. Deformation took place at temperatures of 510–580 °C under low-pressure conditions (0.25–0.45 GPa) and corresponds to the latest stages of pre-Alpine metamorphic evolution. The pre-Alpine mylonitization conditions were close to the brittle-ductile transition, as indicated by syn–mylonitic generation of pseudotachylytes and high differential stress inferred from quartz grain-size piezometry. The brittle-ductile behaviour at a relatively high temperature, and the absence of annealing textures in quartz aggregates, are suggestive of water-deficient conditions during mylonitization. These were accomplished through progressive consumption of water by syn–kinematic hydration reaction and by adsorption onto the greatly increased grain boundary area resulting from dynamic recrystallization.

**Key words:** amphibolite facies metamorphism; brittle-ductile transition; pseudotachylytes; water-deficient mylonites; Western Alps.

## INTRODUCTION

The close relationship between water presence and ductile deformation is supported by structural, petrological and geochemical lines of evidence (e.g. Kerrich, 1986; Segall & Simpson, 1986; Burkhard & Kerrig, 1988; McCaig, 1988; Gibson, 1990; Kronenberg *et al*., 1990; Andersen *et al*.,,. 1991; Tobisch *et al*., 1991; Boundy *et al*., 1992; Fruh-Green, 1994; Pennacchioni, 1996). As $H_2O$ has an enhancing effect on the ductile flow of rocks, zones of localized ductile deformation (mylonites) are commonly assumed or inferred to have developed in the presence of a fluid comprising either pure $H_2O$ (*water*) or an $H_2O$-rich mixture (*aqueous fluid*). For the purpose of this paper, both these situations will be described as *water-present conditions*. However, the presence of an intergranular aqueous fluid is not necessary for the development of mylonites (e.g. Passchier, 1985; Clarke & Norman, 1993), that may also form under *fluid-absent conditions*, or in the presence of $H_2O$-poor mixtures (*$H_2O$-undersaturated*). We refer to both these situations as *water-deficient conditions*.

Experimental studies show that ductile deformation under water-deficient conditions requires higher temperatures than water-present conditions (e.g. Hirth & Tullis, 1992), but experimental data are limited and their geological extrapolation is problematic. The effect of fluid on the rheological characteristics of natural rocks may be inferred if the brittle-ductile transition can be estimated at different temperatures in mylonites which formed with or without $H_2O$. Therefore, the recognition of mylonites that formed close to the brittle-ductile transition and their petrological study is particularly important.

The rocks studied in this work are pre-Alpine mylonites from the Austroalpine Mont Mary nappe (Italian Western Alps). They show textural and mineralogical characters consistent with deformation close to the brittle-ductile transition, by analogy with the water-deficient mylonites described in the Saint-Barthelemy Massif (French Pyrenees) by Passchier (1985). The aim of this paper is to show that initial water-present conditions progressively evolved to water-deficient conditions during the mylonitic event, as a result of the interplay between hydration reactions and deformation processes. The occurrence in the Mont Mary nappe of later, hydrated Alpine mylonites

developed from the same rocks at lower temperature than pre-Alpine mylonite show the possibility of achieving brittle-ductile transition at different temperatures as a result of varying the amount of free $H_2O$ of the rocks during deformation.

## GEOLOGICAL SETTING

In the north-western Alps, the Dent Blanche and Mont Mary basement nappes belong to the upper element of the Austroalpine nappe system (Ballevre *et al.*, 1986), forming the top of the Alpine stack (Fig. 1). They represent a slice of the Adria continental margin involved in the Alpine orogeny (Polino *et al.*, 1990 and refs therein).

The Dent Blanche and Mont Mary nappes are juxtaposed along a major mylonitic zone of Alpine age, which involves Permo-Mesozoic metasedimentary rocks (Roisan Zone *Auct.*). Within each nappe, Alpine mylonitic zones also separate two main tectonic units: the Arolla and Valpelline units (Stutz & Masson, 1938; Diehl *et al.*, 1952). Well preserved pre-Alpine rocks form the largest part of the structurally upper Valpelline unit: they consist of granulite to amphibolite facies metapelites with minor metabasites and marbles (Diehl *et al.*, 1952; Nicot, 1977; Canepa *et al.*, 1990). In the Dent Blanche nappe, the metapelites of the Valpelline unit record a pre-Alpine metamorphic evolution including (Gardien *et al.*, 1994): (i) an early intermediate-pressure granulitic phase (700–750 °C; 0.9–1 GPa); (ii) a decompressional stage with a small increase of temperature (750–800 °C, 0.4–0.6 GPa), followed by the development of the main fabric during slight cooling; (iii) further decompression and cooling (650–700 °C, 0.35–0.45 GPa). According to Gardien *et al.* (1995) the decompressional evolution can be correlated to the extensional regime which finally led to the opening of the Mesozoic Tethys (Lardeaux & Spalla, 1991; Dal Piaz, 1993). A similar pre-Alpine metamorphic evolution may be inferred for the Mont Mary nappe (Canepa *et al.*, 1990).

During the Alpine history, the Dent Blanche and Mont Mary nappes were affected by polyphase deformation (De Leo *et al.*, 1987; Canepa *et al.*, 1990; Pennacchioni & Guermani, 1993), accompanied by a prominent greenschist facies re-equilibration. In the Valpelline unit, the Alpine deformation and metamorphism are strongly localized to mylonitic shear zones, allowing large volumes of pre-Alpine rocks to be preserved.

## PRE-ALPINE MYLONITES IN THE MONT MARY NAPPE

Besides the typical greenschist facies Alpine mylonites of the Dent Blanche and Mont Mary nappes (Canepa *et al.*, 1990; Pennacchioni & Guermani, 1993), another type of mylonites can be recognized in the Valpelline unit of the Mont Mary nappe (Masson, 1938; Diehl *et al.*, 1952; Canepa *et al.*, 1990). These mylonites are pre-Alpine in age as discussed later and will be referred hereafter as pre-Alpine mylonites.

The pre-Alpine mylonites are derived from biotite-rich metapelites and occur in one main horizon that ranges in thickness from a few metres to over 30 m and may be traced for a few kilometres. In the field, the pre-Alpine mylonites are dark-brown to black (ultramylonites), and contain macroscopic porphyroclasts of garnet and plagioclase. Despite having a well developed, closely spaced foliation, they do not show a good cleavage and are characterized by a splintery fracture (ultramylonites). The mineral stretching lineations within these pre-Alpine mylonites trend NE-SW. By contrast, the Alpine mylonites are grey-greenish, have a strong rock cleavage, are free of relics of garnet and feldspar, and their mineral stretching lineations trend NW-SE.

The *protoliths* of the pre-Alpine mylonites are coarse-

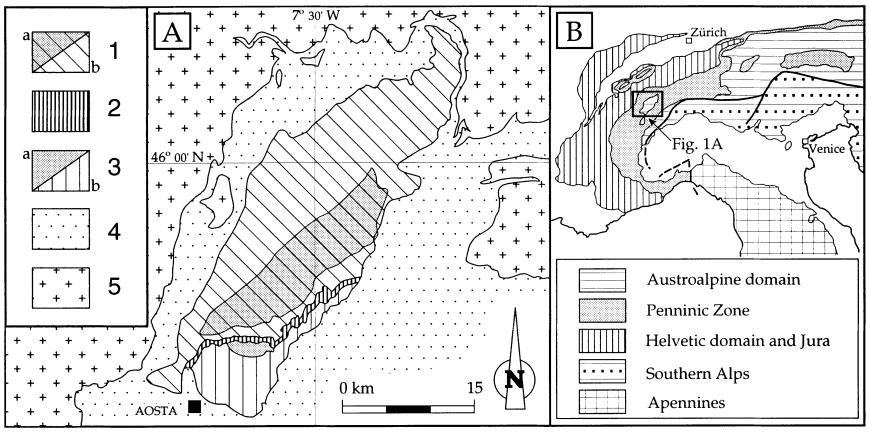


**Fig. 1.** (A) Tectonic map of the Dent Blanche and Mont Mary nappe region. (1) Dent Blanche nappe: (a) upper tectonic unit (Valpelline unit); (b) lower tectonic unit (Arolla unit); (2) Roisan Zone; (3) Mont Mary nappe: (a) upper tectonic unit; (b) lower tectonic unit; (4) Piedmont ophiolitic nappes; (5) Penninic basement nappes. (B) Location of the map in the Alpine belt.

grained metapelites consisting of quartz, garnet$_1$, sillimanite, biotite$_1$, plagioclase$_1$, K-feldspar, ilmenite$_1$, graphite $\pm$ cordierite (where the subscript 1 refers to the pre-Alpine protolith phases). A compositional banding of quartz-feldspar layers and biotite–sillimanite-rich folia, anastomosing around porphyroblastic garnet, outlines the foliation, which is locally cut by quartz–feldspar pegmatitic veins and dykes. Mylonitic deformation variably affected these rocks with progressive development, under increasing strain, of protomylonite to ultramylonite.

The *protomylonites* have a lenticular fabric, in which a dark, biotite-rich matrix and quartz ribbons anastomose around garnet porphyroclasts and lens-shaped feldspar-rich domains; the latter are partly derived from transposition of pegmatites. An incipient, centimetre-spaced, shear-band cleavage is commonly present (Fig. 2a).

The *mylonites* and *ultramylonites* are matrix-dominated, ultrafine-grained rocks. The ultramylonites show a well-developed submillimetric planar fabric (Fig. 2b), outlined by thin layers and ribbons of feldspar and quartz and by the colour striping of the matrix, which includes black to light brown layers. A mineral stretching lineation is visible in quartz and feldspar layers although not in the matrix; it is parallel to the fold axes of syn-mylonitic folds. Mesoscopic shear bands are absent. In contrast to the protomylonites, biotite porphyroclasts are not present in the mylonites and ultramylonites, whereas garnet and feldspar still occur, although their amount and grain-size are greatly decreased.

*Pseudotachylites* are locally present in the mylonites–ultramylonites. They consist of dark aphanitic veins that are commonly found in fault vein-injection vein arrays (Sibson, 1975; Swanson, 1992), where foliation-parallel veins show apophyses intruding at high angle to the foliation (Fig. 2c); the veins may reach 1 cm in thickness (fault veins), but are typically a few millimetres thick. Some fault surfaces are only discontinuously outlined by small pseudotachylite veins, representing small pull aparts associated with steps in the fault plane. Pseudotachylites locally occur in

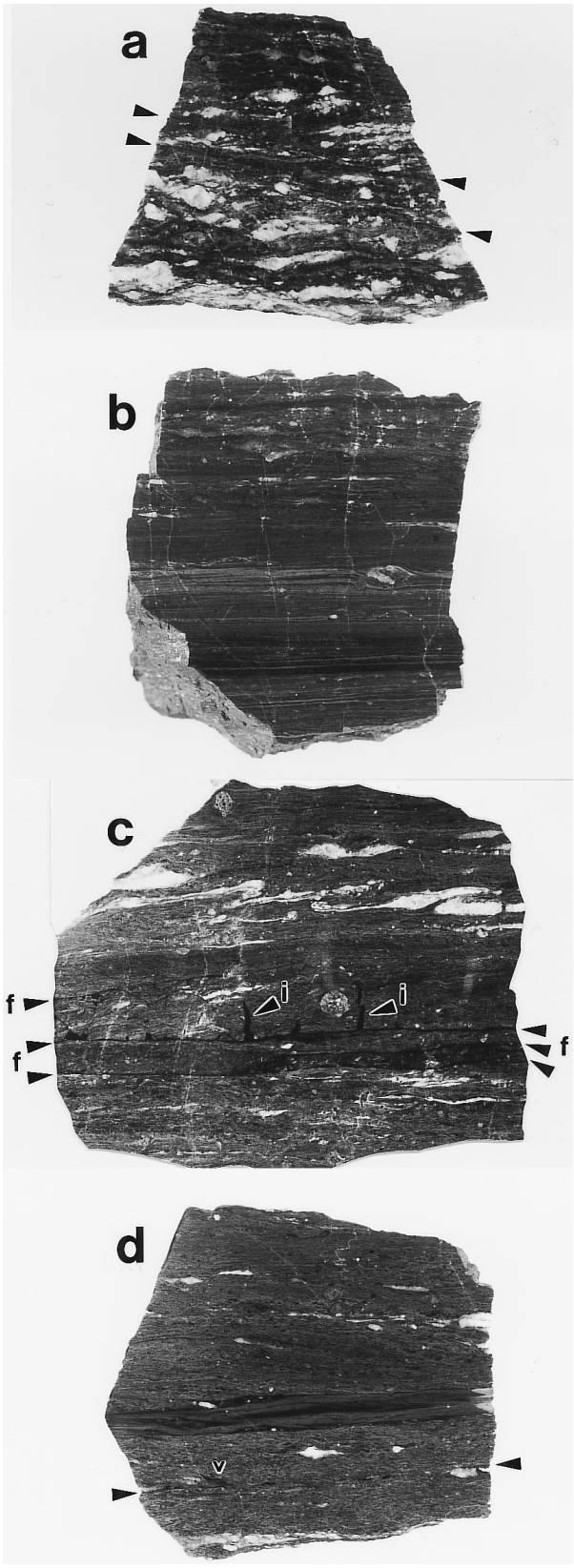


**Fig. 2.** Polished samples of pre-Alpine mylonites of the Mont Mary nappe. (a) Protomylonite: biotite-rich matrix, anastomosing around quartz-feldspar lenses, cut by spaced shear bands (arrows); (b) Transition from mylonitic (upper part of the sample) to a planar, finely layered ultramylonitic fabric (central and lower part); (c) 'Pseudotachylite generation zones': the pseudotachylytes (black) consist of pairs of overlapping layer-parallel fault veins (f) and a network of injection veins (i) in between. The latter include orthogonal dilatant veins and conjugate shear fractures. (d) Centimetre-thick aphanitic band, with internal flow structure and folding, slightly discordant to the mylonitic foliation. It is subparallel to the adjacent pseudotachylyte-bearing fault plane (arrows) which is discontinuously lined by pseudotachylites and shows a small injection vein (v) in the mylonitic foliation. The sample (maximum) widths are: 8 cm (a), 7 cm (b), 10 cm (c) and 8.5 cm (d).

'pseudotachylite generation zones' (Fig. 2c; Grocott, 1981; Swanson, 1992), which include dilatant veins and conjugate shear fractures between pairs of overlapping fault veins. The mylonites also include some aphanitic bands, lying subparallel to the mylonitic foliation and showing internal flow structure and folding (Fig. 2d), which have been recognized to be ductilely deformed pseudotachylites by microscopic analysis.

## MICROSTRUCTURES

A main characteristic of the pre-Alpine mylonites–ultramylonites is the abundance of porphyroclasts of garnet, plagioclase and sillimanite (Fig. 3). Although porphyroclasts decrease in amount and size with increasing strain they are still abundant (commonly >10 volume percentage) in rocks showing a deformation-induced, finely layered fabric (ultramylonites). The σ- and δ-type porphyroclast systems and other micro-

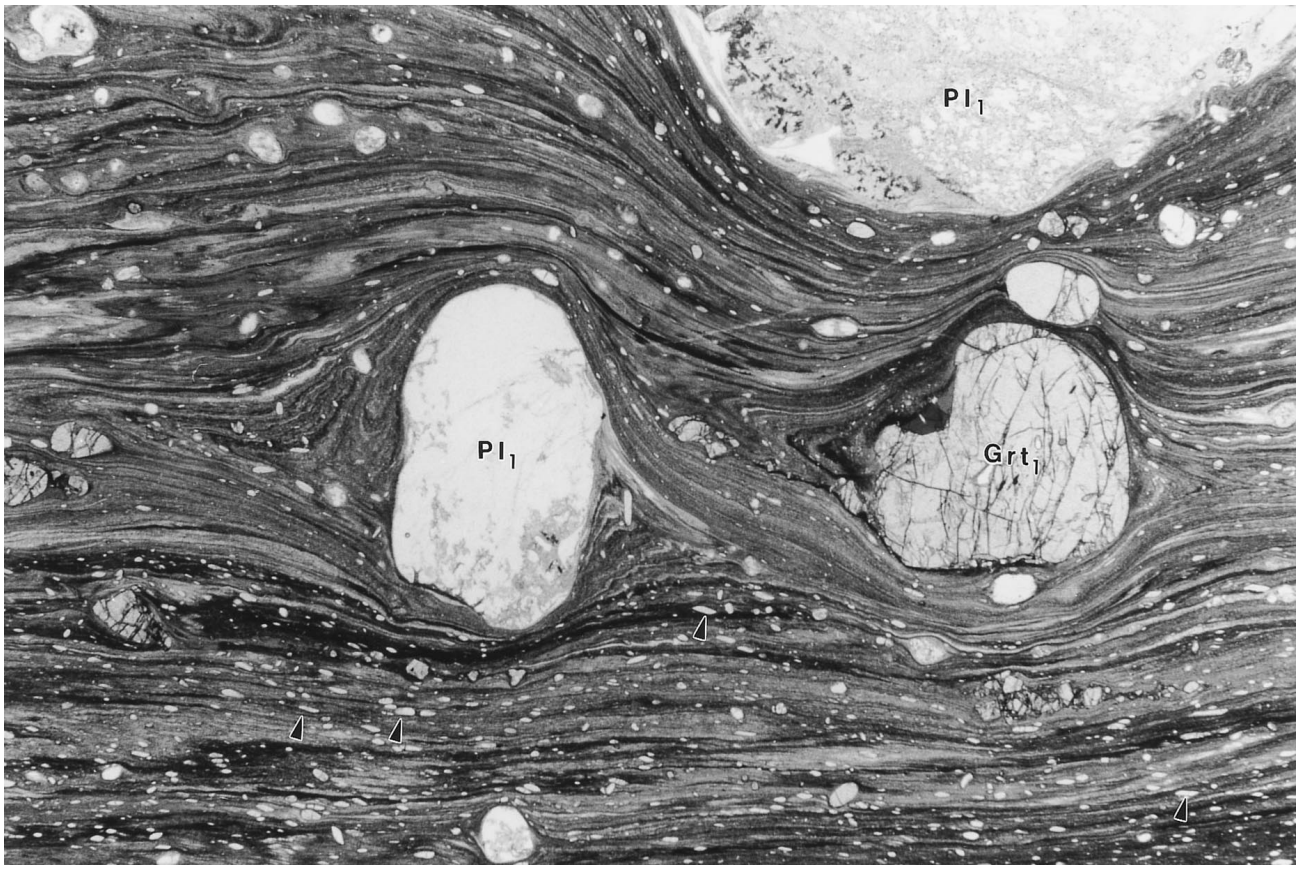


**Fig. 3.** Typical microscopic appearance of a pre-Alpine ultramylonite. The matrix has a finely layered structure, outlined by colour striping, and contains porphyroclasts of garnet ($Grt_1$), plagioclase ($Pl_1$), and sillimanite (white, small prismatic-rhomboid grains, arrows), abundant in the lower part of the figure. The presence of porphyroclasts produces distortion in the matrix flow and generates an asymmetric fabric useful to deduce the sense of shear (sinistral in the present case). Plane-polarized light (N//); width of view (w): 10 mm.

**Fig. 4.** (a) Backscattered electron microscope (BSEM) image of the mylonite matrix consisting of biotite$_2$ (Bt: light gray), muscovite (Ms: dark gray), quartz$_2$ and sillimanite (Qtz, Sil: black), ilmenite$_2$ (Ilm: white) and isolated euhedral crystals of garnet (Grt: white); (b) Deformation bands in quartz$_1$ of a protomylonite with irregular boundary morphology. Subgrains and incipient fine recrystallization occur within some deformation bands. Crossed polars (NX); w = 0.6 mm; (c) Reflected light micrograph of the etched surface of a quartz$_2$ aggregate in a mylonite (sample used for grain-size measurement). Quartz$_2$ shows a preferred elongation of quartz grains inclined with respect to the mylonitic foliation (parallel to the base of the photo). N//; w = 0.29 mm; (d) Biotite$_1$ porphyroclasts (Bt$_1$) surrounded by turbid, fine-grained, biotite$_2$ + ilmenite$_2$ matrix. N//; w = 1.35 mm; (e) Elliptical garnet$_1$ porphyroclasts in a mylonite showing a core zone (encircled by the dashed line) rich in inclusions of quartz, biotite and ilmenite, truncated against the foliation. N//; w = 5 mm; (f) 'Winged' garnet$_1$ porphyroclasts with tails of fine-grained biotite$_2$ (light gray). N//; w = 3.4 mm; (g) Small euhedral garnet$_2$ with relict core of garnet$_1$ inside an ultramylonite; note the abundance of sillimanite in the matrix. N//; w = 1.35 mm. (h) BSEM image of garnet$_2$ coronas around garnet$_1$ porphyroclasts. The inclusion-rich (ilmenite$_2$ and quartz$_2$) zone marks the boundary between the two garnet generations.

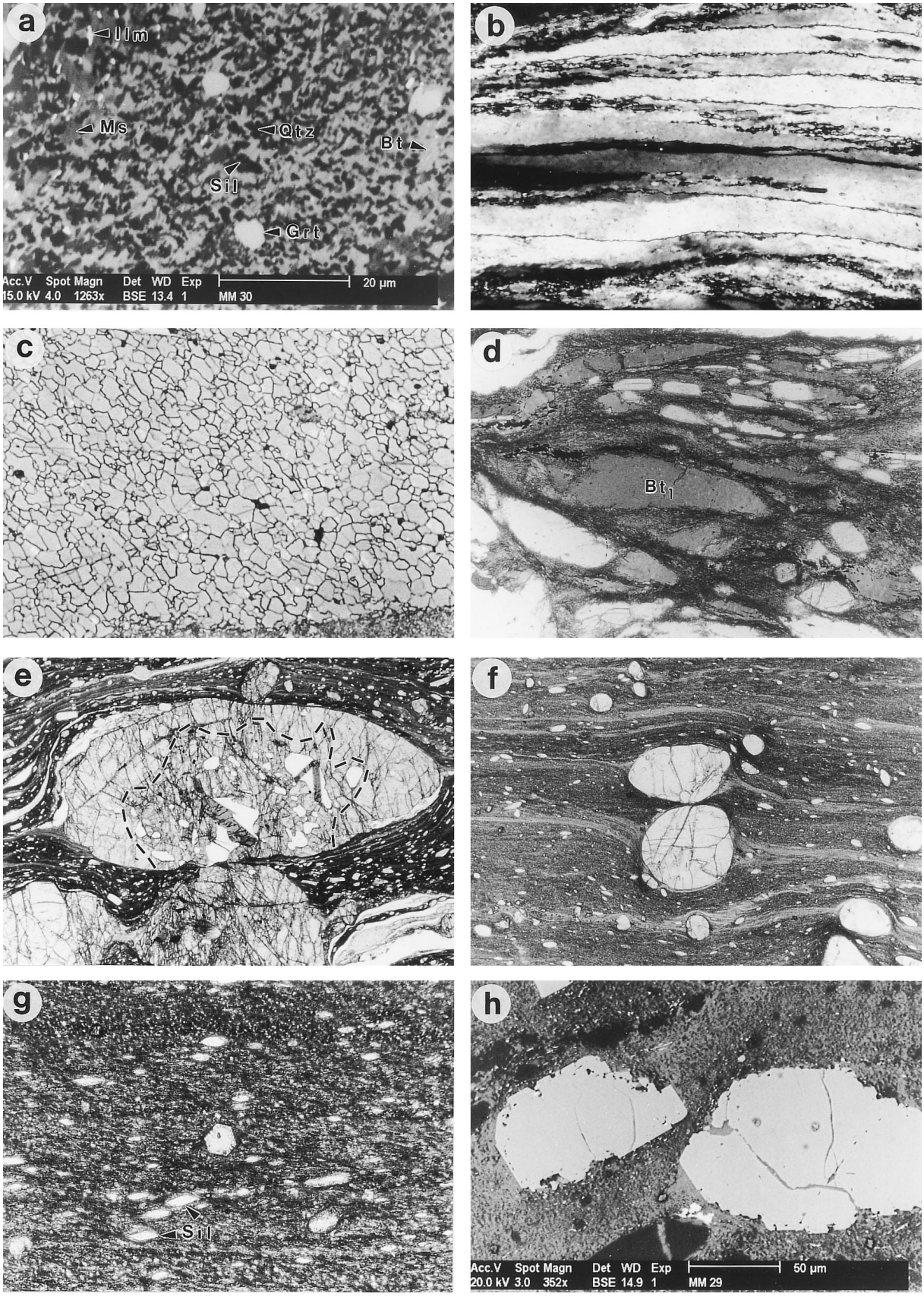
a
Ilm
Ms
Qtz
Bt
Sil
Grt
Acc.V Spot Magn Det WD Exp
15.0 kV 4.0 1263x BSE 13.4 1 MM 30
20 µm
b
c
d
Bt1
e
f
g
Sil
h
Acc.V Spot Magn Det WD Exp
20.0 kV 3.0 352x BSE 14.9 1 MM 29
50 µm

scopic fabric elements have strong monoclinic symmetry and indicate non-coaxial flow during mylonitization. In the following section, we describe microstructural features of the mylonites, in order to infer the stable syn-kinematic assemblage to be used for the petrological analysis and for estimation of the $P$–$T$ and stress conditions of mylonitization.

### Matrix

Under the microscope, the dark matrix of the mylonites is a turbid ultrafine-grained aggregate; it displays homogeneous extinction and pleochroism, suggesting that it is dominated by strongly orientated biotite. The matrix was largely derived by the syn-kinematic recrystallization of biotite$_1$: coupled backscattered electron microscope imaging (Fig. 4a) and microanalysis show that it is composed of biotite$_2$ (average grain-size of 1–5 $\mu$m) with additional ilmenite$_2$, quartz$_2$, muscovite and graphite (where the subscript 2 refers to the pre-Alpine syn-mylonitic minerals). The biotite-rich matrix of the ultramylonites frequently shows a microscopic shear-band cleavage.

### Quartz

Coarse-grained quartz of the protolith (quartz$_1$) is deformed into lenticular domains and ribbons during mylonitization. In protomylonites, relict quartz$_1$ is characterized by undulose extinction, deformation bands, subgrains (Fig. 4b) and deformation lamellae. Even in rocks showing evidence of relatively high plastic strain, as indicated by microboudinage of sillimanite needle inclusions, quartz generally shows limited recrystallization into fine-grained aggregates (quartz$_2$). Recrystallization is localized within thin, foliation-parallel seams and deformation-band boundaries. Deformation banding includes low-mismatched domains and kink bands, with parallel-sided to lenticular morphology. The deformation-band boundaries are parallel to the foliation and range in morphology from smooth to irregular-lobate (Fig. 4b).

With increasing strain, the number of progressively thinner deformation bands increases, as well as the extent of recrystallization. In the mylonites, quartz layers still include monocrystalline ribbons alternating with dynamically recrystallized aggregates, which may display extinction banding inherited from a former deformation banding structure. Quartz$_2$ aggregates display a strong crystallographic preferred orientation and commonly a shape preferred orientation (Fig. 4c). The long axes of quartz$_2$ grains range from oblique to parallel to the mylonitic foliation. The presence of optically visible deformation lamellae and subgrains and the persistence, up to high strain, of high aspect ratio original grains are characteristic of quartz deformation in regime 2 of dislocation creep (Hirth & Tullis, 1992), where the recrystallization occurs predominantly by subgrain rotation. The presence of lobate grain boundaries of quartz$_2$ and their diffuse preservation indicates that grain boundary migration recrystallization also occurred and that there was no significant post-kinematic annealing.

The grain-size of quartz$_2$ aggregates derived from complete recrystallization of quartz$_1$ has been measured in a mylonite and ultramylonite sample using the linear intercept method of Smith & Guttmann (1953), on etched polished surfaces (Ord & Christie, 1984). To avoid the effects of a second phase (Hobbs *et al*., 1976), only monomineralic quartz layers were measured. The recrystallized grain-sizes were derived from an average of 3200 intercepts measured along lines in three mutually perpendicular directions, in order to take into account the grain shape of quartz$_2$; for details see Christie & Ord (1980). The mean grain-size of quartz$_2$ is 5.6 μm in the ultramylonite and 9.6 $\mu$m in the mylonite.

### Biotite

Millimetre-sized red-brown biotite$_1$ occurs in protomylonites as dissected relics showing mantle replacement by fine-grained biotite$_2$ + ilmenite$_2$ aggregates (Fig. 4d). In mylonites, biotite$_1$ forms rare asymmetric mica-fish. Biotite$_2$ is the main component of the mylonite matrix and derives from both dynamic recrystallization of biotite$_1$ and alteration of garnet. The biotite$_2$ derived from garnet does not show the turbid appearance (owing to ilmenite$_2$ disseminations) that is typical of the matrix derived from biotite$_1$.

### Garnet

In the weakly deformed rocks, garnet$_1$ occurs as round to slightly elliptical porphyroclasts up to 1 cm in size, with cores rich in quartz, biotite, sillimanite and ilmenite inclusions. The ellipticity of garnet$_1$ increases with strain, owing to dissolution along the surfaces facing the foliation, as indicated by the truncation of the inclusion-rich cores (Fig. 4e). Grain-size reduction of garnet porphyroclasts occurs mainly by cataclasis: fractures are arranged randomly, in locally pervasive networks, or in sets orientated at a high angle to the foliation, producing book-shelf structures. During cataclasis, biotite-filled garnet fractures acted as soft matrix and assisted deformation of garnet to lenticular domains.

In the ultramylonites, garnet$_1$ occurs in σ-type porphyroclast systems (Passchier & Simpson, 1986) composed of small garnet porphyroclasts with tails of reaction-softened, fine-grained aggregates of biotite$_2$ extending into the foliation (Fig. 4f). Ultramylonites also contain a second generation of garnet (garnet$_2$), either as euhedral small crystals ($<80$ $\mu$m in diameter) scattered in the matrix (Fig. 4 g) or as a narrow corona (30–40 $\mu$m in thickness) around garnet$_1$ porphyroclasts (Fig. 4 h). Garnet$_2$ coronas commonly contain micron-sized inclusions of matrix quartz and ilmenite$_2$: this texture suggests that garnet$_2$ coronas formed by

overgrowth, rather than replacement, of garnet$_1$. A syn-kinematic growth of garnet$_2$ is suggested by the presence of pressure shadows and wrapping of the matrix around small euhedral grains of garnet$_2$ (Fig. 5a), free of core relics of garnet$_1$, and by the pattern of the matrix inclusions in garnet$_2$.

### Feldspar

In the protomylonites, millimetre-sized plagioclase$_1$ porphyroclasts show undulose extinction and recrystallization to very fine-grained (average grain-size $< 5\,\mu m$) aggregates of plagioclase$_2$. Recrystallization occurs along microshear zones, microfractures and at grain mantles. Microshear zones and fractures are arranged subparallel and at high angles to the mylonitic foliation, locally defining conjugate sets or extensional shear bands. High strain results in: (i) widening of microshear zones, (ii) nucleation of new ones, and (iii) displacement of plagioclase fragments along fine-grained recrystallization aggregates.

In the mylonites, plagioclase is the most abundant feldspar, K-feldspar being almost completely absent. In the mylonites, there are lenticular-ribbon domains of recrystallized plagioclase$_2$ which include a few small clasts of plagioclase$_1$. In ultramylonites, plagioclase$_1$ occurs as isolated round to elliptical porphyroclasts (Fig. 5b) surrounded by asymmetric δ- to complex-shaped recrystallized mantles (Fig. 5c, d; Passchier & Simpson, 1986). Deformation microstructures in plagioclase are locally obscured by the Alpine saussuritization.

### Sillimanite

In the protolith, sillimanite occurs as large prismatic crystals, isolated or grouped in folia interleaved with biotite. During mylonitization, sillimanite is microboudinaged or microfolded without showing any recovery texture or recrystallization. Boudin necks and pressure shadows of sillimanite are filled with biotite$_2$ (Fig. 5e) and graphite. In the ultramylonites, sillimanite is still very abundant and shows preferred shape orientation oblique to the mylonitic layering (Fig. 3), resulting from back-rotation (Hanmer, 1986) during the development of shear bands. Dissolution along the shear bands gave rise to rhomboid-shaped sillimanite (Figs 3 & 4g). The abundance of sillimanite in the ultramylonites (Figs 3 & 4g), and the absence of replacement by other $Al_2SiO_5$ polymorphs or by 'shimmer aggregates' of muscovite (Fig. 5e), point to the stability of sillimanite in the mylonites. Local muscovite coronas are post-kinematic and have probably developed during the Alpine greenschist facies overprint.

### Pseudotachylites

Pseudotachylites unaffected by ductile deformation (Fig. 5f) consist of a recrystallized isotropic groundmass of randomly orientated, fine-grained biotite and euhedral ilmenite, including angular clasts (mainly quartz) from the host mylonite. No glass has been observed, but ilmenite commonly defines a globular texture, with a mean diameter of globules of a few microns (Fig. 5g), which probably derives from devitrification. A flow banding including dark and lighter bands is locally present and is folded in some injection veins. The pseudotachylite veins commonly show opaque borders (Fig. 5h), owing to concentration of ilmenite and graphite, and a cataclastic deformation of the surrounding mylonite (Fig. 5f).

Most pseudotachylites were later folded and/or foliated. In deformed pseudotachylites, the foliation is defined by the preferred orientation of matrix biotite (present from the early stages of ductile overprint: Fig. 5i), by ilmenite trails, and by the shape fabric of flattened and recrystallized quartz lenses (Fig. 5l); the rare sillimanite and garnet clasts have biotite pressure shadows. During the ductile overprint of pseudotachylites, the mylonitic assemblage stably persists and therefore pseudotachylites are inferred to have formed under the same metamorphic conditions as the host mylonites.

The product of intense ductile deformation of pseudotachylites (see Fig. 2d) may resemble ultramylonites. However, distinguishing features of deformed pseudotachylites are: (i) the sharp boundaries with the host mylonites; (ii) the occurrence of cataclastic deformation of the host mylonite; (iii) the rarity of garnet, plagioclase and sillimanite porphyroclasts; (iv) the low aspect ratio of quartz lenses derived from quartz fragments.

## MINERAL CHEMISTRY

The chemical compositions of garnet, biotite and plagioclase from a mylonite (MM29) and an ultramylonite (MM30) were analysed using a Cameca Camebax electron microprobe (EMP) of CNR at the Department of Mineralogy and Petrology of the University of Padova. In order to verify the quality of the EMP data, and to test for contamination by adjacent grains of other minerals, the matrix micron-sized biotite$_2$ was also analysed by Analytical Electron Microscopy (AEM) at the Department of Earth Science of the University of Siena. This technique (Peacor, 1992) utilizes an energy dispersive spectrometer (EDS) combined with a transmission electron microscope (TEM). Although the AEM data have a semiquantitative precision, coupled EMP and AEM analyses on large biotite$_1$ porphyroclasts allow the AEM technique to be comparatively calibrated. Mineral compositions are reported in Table 1.

### Garnet

With respect to garnet$_1$ ($Alm_{78-79}Sps_{2-3}Pyp_{15}Grs_4$), garnet$_2$ is characterized by higher spessartine (3–5%)

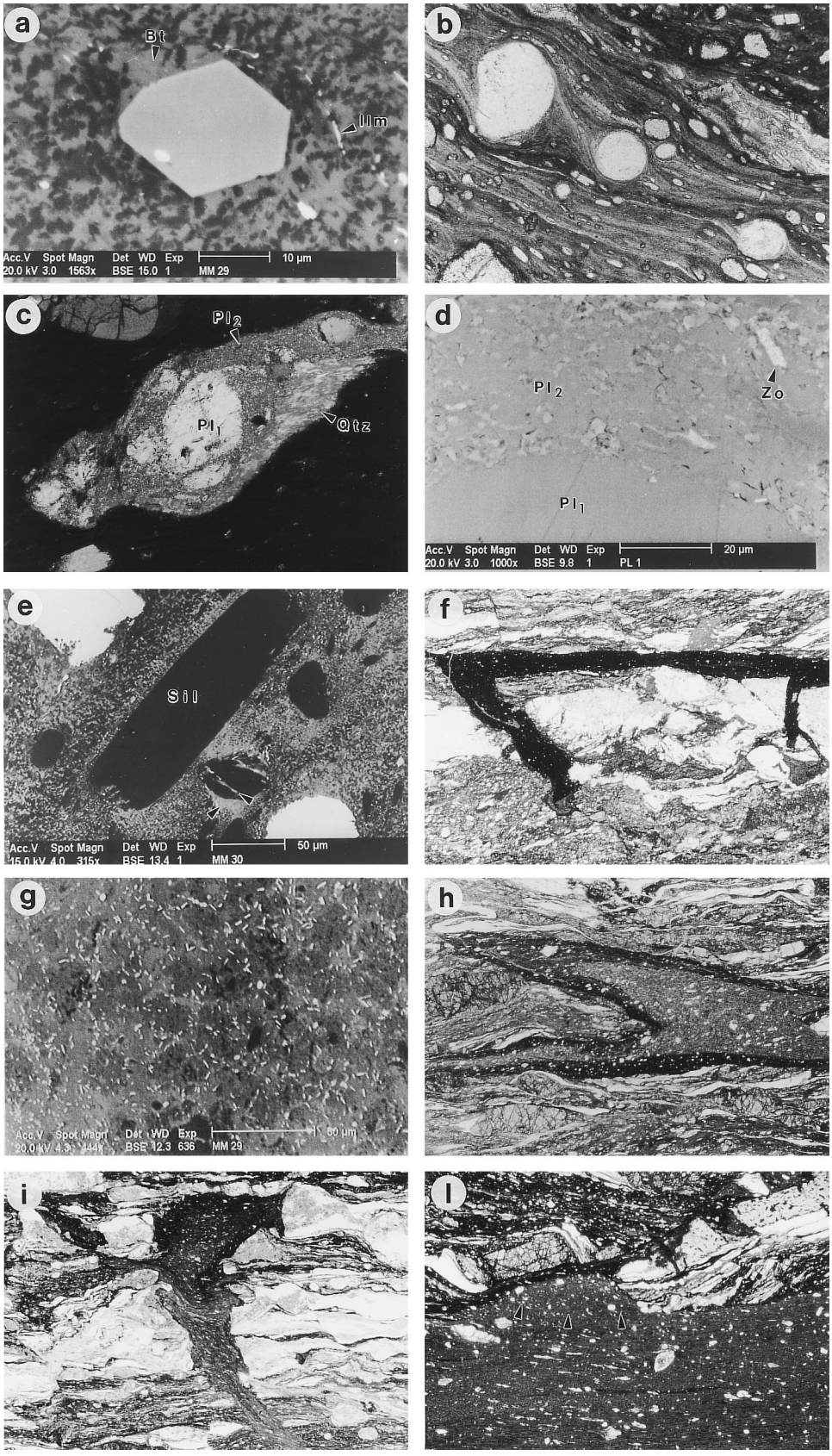
a
Bt
Ilm
Acc.V Spot Magn Det WD Exp 10 µm
20.0 kV 3.0 1563x BSE 15.0 1 MM 29
b
c
Pl2
Pl1
Qtz
d
Pl2
Zo
Pl1
Acc.V Spot Magn Det WD Exp 20 µm
20.0 kV 3.0 1000x BSE 9.8 1 PL 1
e
Sil
Acc.V Spot Magn Det WD Exp 50 µm
15.0 kV 4.0 315x BSE 13.4 1 MM 30
f
g
Acc.V Spot Magn Det WD Exp 50 µm
20.0 kV 4.3 444x BSE 12.3 636 MM 29
h
i
l

**Table 1.** Electron microprobe analyses (average of *n* spots) of garnet, biotite and plagioclase, normalized on the basis of 24, 22 (anhydrous), and 8 oxygens, respectively. Total iron as FeO. Alm = Fe/(Fe + Mg + Mn + Ca). Sps = Mn/(Fe + Mg − Mn + Ca). Py = Mg/(Fe + Mg + Mn + Ca). Grs = Ca/(Fe + Mg + Mn + Ca); $X_{Fe}$ = Fe/(Fe + Mg). An = Ca/(Na + Ca).

| | Garnet | | | | | Biotite | | | | | Plagioclase | | | | |
|---|---|---|---|---|---|---|---|---|---|---|---|---|---|---|---|
| Analysis | 1 | 2 | 3 | 4 | Analysis | 5 | 6 | 7 | 8 | Analysis | 9 | 10 | 11 | 12 | 13 |
| Sample | MM29 | MM29 | MM30 | MM30 | Sample | MM29 | MM29 | MM30 | MM30 | Sample | MM29 | MM29 | MM30 | MM30 | MM30 |
| n | 24 | 18 | 22 | 15 | n | 3 | 1 | 1 | 1 | n | 1 | 1 | 6 | 6 | 1 |
| | Grt1 | Grt2 | Grt1 | Grt2 | | Bt1 | Bt2 | Bt1 | Bt2 | | Pl1 | Pl2 | Pl1 | Pl2 | |
| MgO | 3.93 | 2.82 | 3.66 | 2.38 | MnO | 0.01 | 0.07 | 0.08 | 0.00 | $SiO_2$ | 59.88 | 59.02 | 60.10 | 60.88 | 62.19 |
| FeO | 35.40 | 36.56 | 35.20 | 35.48 | $Al_2O_3$ | 17.27 | 18.82 | 17.33 | 22.36 | $Al_2O_3$ | 25.74 | 25.86 | 25.66 | 25.54 | 24.50 |
| MnO | 1.01 | 1.43 | 1.14 | 2.20 | FeO | 18.41 | 18.89 | 17.78 | 19.14 | CaO | 7.34 | 7.36 | 7.26 | 7.36 | 5.41 |
| $SiO_2$ | 37.58 | 37.36 | 37.24 | 36.97 | $SiO_2$ | 35.53 | 34.95 | 35.55 | 36.52 | $Na_2O$ | 7.08 | 7.46 | 7.60 | 7.50 | 8.41 |
| $Al_2O_3$ | 21.10 | 20.92 | 20.85 | 20.83 | $TiO_2$ | 4.67 | 2.37 | 4.44 | 2.17 | $K_2O$ | 0.16 | 0.21 | 0.14 | 0.05 | 0.01 |
| CaO | 1.48 | 1.47 | 1.43 | 1.38 | MgO | 9.84 | 9.89 | 9.90 | 7.58 | Total | 100.20 | 99.91 | 100.76 | 101.35 | 100.53 |
| Total | 100.50 | 100.56 | 99.52 | 99.24 | $Na_2O$ | 0.21 | 0.11 | 0.22 | 0.13 | | | | | | |
| Mn | 0.14 | 0.19 | 0.16 | 0.30 | $Al^{IV}$ | 2.60 | 2.63 | 2.58 | 2.60 | Si | 2.66 | 2.64 | 2.66 | 2.67 | 2.74 |
| Al | 3.96 | 3.96 | 3.97 | 3.99 | | | | | | Al | 1.35 | 1.36 | 1.34 | 1.32 | 1.27 |
| Fe | 4.72 | 4.91 | 4.75 | 4.83 | Si | 5.40 | 5.37 | 5.42 | 5.40 | Ca | 0.35 | 0.35 | 0.34 | 0.35 | 0.26 |
| | | | | | $K_2O$ | 9.13 | 8.84 | 9.18 | 8.48 | Na | 0.61 | 0.65 | 0.65 | 0.64 | 0.72 |
| Si | 6.00 | 6.00 | 6.01 | 6.02 | Total | 95.07 | 93.94 | 94.48 | 96.38 | K | 0.01 | 0.01 | 0.01 | 0.00 | 0.00 |
| Mg | 0.93 | 0.67 | 0.88 | 0.58 | $Al^{VI}$ | 0.50 | 0.78 | 0.53 | 1.03 | | | | | | |
| Ca | 0.25 | 0.25 | 0.25 | 0.24 | Ti | 0.53 | 0.27 | 0.51 | 0.24 | An | 0.36 | 0.35 | 0.35 | 0.35 | 0.26 |
| | | | | | Fe | 2.34 | 2.43 | 2.27 | 2.37 | | | | | | |
| Alm | 0.78 | 0.81 | 0.79 | 0.81 | Mn | 0.00 | 0.01 | 0.01 | 0.00 | | | | | | |
| Sps | 0.02 | 0.03 | 0.03 | 0.05 | Mg | 2.23 | 2.27 | 2.25 | 1.67 | | | | | | |
| Pyp. | 0.15 | 0.11 | 0.15 | 0.10 | Na | 0.06 | 0.03 | 0.06 | 0.04 | | | | | | |
| Grs | 0.04 | 0.04 | 0.04 | 0.04 | K | 1.77 | 1.73 | 1.78 | 1.60 | | | | | | |
| | | | | | $X_{Fe}$ | 0.51 | 0.52 | 0.50 | 0.59 | | | | | | |

and almandine (81%), and lower pyrope (10–11%) contents; the chemical differences between $garnet_1$ and $garnet_2$ are more pronounced in the ultramylonite. Coronas and euhedral crystals of $garnet_2$ have the same composition. Chemical profiles across garnet crystals indicate that: (i) the $garnet_2$ coronas are continuous and have a thickness of 30–40 $\mu$m, and (ii) the euhedral $garnet_2$ in the matrix shows a homogeneous composition where its diameter is less than 50–70 $\mu$m; otherwise it contains a relict core of $garnet_1$.

### Biotite

$Biotite_1$ is Ti-rich (0.51–0.53 atoms p.f.u.), aluminous, and has $X_{Fe}$ in the range 0.50–0.51. EMP analyses of $biotite_2$, consistent with AEM data, indicate markedly lower Ti and higher Al and $X_{Fe}$ than $biotite_1$. TEM analysis also demonstrates that $biotite_2$ is homogeneous and does not contain submicroscopic intergrowths of

### Plagioclase

In both the mylonite and ultramylonite samples, $plagioclase_1$ and $plagioclase_2$ have a very similar composition: $An_{35\pm1}$ and $An_{35\pm2}$, respectively. More albitic compositions ($An_{26}$: analysis 13 in Table 1) have been detected where [illegible] is present (Fig. 5d) as a

## MYLONITIZATION CONDITIONS

### Mineral reactions

Microstructural analysis indicates that the ultramy-

**Fig. 5.** (a) BSEM image of an euhedral crystal of $garnet_2$ showing biotite-rich pressure shadows. The mylonitic foliation, lined by ilmenite, wraps around the garnet; (b) δ-shaped plagioclase porphyroclasts in a ultramylonite. N//; w = 1.35 mm; (c) Mantle of recrystallized $plagioclase_2$ ($Pl_2$) around a porphyroclast of $plagioclase_1$ ($Pl_1$). NX; w = 1.35 mm; (d) BSEM detail of the recrystallization mantle of $plagioclase_2$ around $plagioclase_1$ porphyroclast: brightest crystals are zoisite (Zo); (e) BSEM image of sillimanite porphyroclasts (black). Sillimanite is fresh and does not show replacement textures; in places it is microboudinaged with fractures (and pressure shadows) filled with $biotite_2$ (arrows) (f) Undeformed pseudotachylyte including a layer-parallel fault vein and intrusion veins. The small spots in the black pseudotachylyte groundmass are clasts of quartz. Note the brittle deformation of the mylonite fabric, which is almost completely disrupted in the bottom part of the photo. N//; w = 7.5 mm. (g) BSEM image of an undeformed pseudotachylyte. Ilmenite crystallites are randomly orientated around unidentified 'globular' Si–Al–Fe–K– bearing phase; (h) Opaque borders of a pseudotachylyte veinlet, rich in graphite and ilmenite. The matrix of the pseudotachylyte shows homogeneous extinction and pleochroism. N//; w = 6.7 mm; (i) Slightly deformed pseudotachylyte intrusion vein; although the intrusive geometry of the vein is still retained, the pseudotachylyte already shows a foliated fabric. N//; w = 12 mm. (l) Ductilely deformed pseudotachylyte vein. The primary, isotropic fabric of the pseudotachylyte, containing equant angular fragments of quartz, is preserved in the embayment (arrows) close to the vein border. The remaining part of the pseudotachylyte vein is foliated, and quartz fragments occur as flattened porphyroclasts. Note the cataclasis of the mylonitic fabric at the margin of the pseudotachylyte vein. N//; w = 6.7 mm.

lonitic assemblage is $Grt_2$–$Bt_2$–Sil–$Pl_2$–Ms–$Qtz_2$–$Ilm_2$–Gph; it developed from the pre-mylonitic $Grt_1$–$Bt_1$–Kfs–Sil–$Qtz_1$–$Pl_1$–$Ilm_1$–Gph paragenesis. The new assemblage is characterized by the appearance of muscovite and consumption of K-feldspar, by compositional changes of biotite and garnet, and by the persistence of sillimanite. The syn–mylonitic stability of sillimanite, accepted throughout the following sections, is suggested by the microstructural relationships and supported by petrological indicators such as: (i) the chemical variations of biotite (increase of Al and decrease of Ti), that are in good agreement with the change from the 'second sillimanite' Kfs + Sil + Qtz to the Ms + Sil + Qtz limiting assemblage, as discussed by Guidotti (1984), and (ii) the temperature estimates in the ultramylonites (see below) that are compatible with sillimanite stability.

Although the syn–mylonitic assemblage has been determined, the participation of the different minerals in the reactions (i.e. their role as reactants or products) is more complex. The possible mass balance relationships have been investigated by matrix analysis using the method of Fisher (1989), with a six-component (Si, Al, Fe, Mg, Ti, K), nine-phase ($Bt_1$–$Grt_1$–Kfs–$Bt_2$–$Grt_2$–Ms–Ilm–Qtz–Sil) matrix, and searching for incompatibilities that contain the assemblage $Grt_1$–$Bt_1$ (± Kfs) as reactants. All the incompatibilities have (a) higher stoichiometric coefficients for garnet as a reactant ($Grt_1$); (b) higher stoichiometric coefficients for biotite as a product ($Bt_2$); (c) quartz and ilmenite as products; (d) muscovite as product when K-feldspar occurs as reactant; (e) muscovite as reactant in Kfs-absent reactions; (f) very low coefficients for sillimanite as product or reactant phase, depending on the presence of K-feldspar. Because of the uncertainties related to the assumed stoichiometry of muscovite, K-feldspar and ilmenite compositions, the results can be summarized by the two qualitative reactions

$$H_2O + Grt_1 + Bt_1 + Kfs = Grt_2 + Bt_2 + Ilm + Qtz + Ms \pm Sil \quad \text{(Kfs-bearing)} \tag{1}$$

$$Grt_1 + Bt_1 + Ms \pm Sil = Grt_2 + Bt_2 + Ilm + Qtz \quad \text{(Kfs-free)} \tag{2}$$

that can be also written in the form

$$H_2O + Grt + Kfs = Bt + Ilm + Qtz + Ms \pm Sil \quad \text{(Kfs-bearing)} \tag{1a}$$

$$Grt + Ms \pm Sil = Bt + Ilm + Qtz \quad \text{(Kfs-free)} \tag{2a}$$

from which it is apparent that, although garnet recrystallizes, its bulk amount is reduced, and new biotite is produced.

Because the pre-mylonitic assemblage contains K-feldspar, but does not contain muscovite, we favour reaction (1) as a model for mylonite formation. This reaction involves $H_2O$ as a reactant for the production of biotite and muscovite. The fluid-absent reaction (2) may have intervened in high-strain domains after consumption of K-feldspar or $H_2O$.

The above net reactions are obtained by mass-balance calculations and might represent the reactions that occurred in the ultramylonites only in the limit of equilibrium. However, they are more likely to represent either (a) a one-step disequilibrium transition from the $Bt_1$–$Grt_1$–Sil–Kfs–Qtz–Ilm to the $Bt_2$–$Grt_2$–Sil–Ms–Qtz–Ilm assemblages, or (b) relicts of the series of stable AFM reactions that would occur with falling temperature in an equilibrium system, i.e.:

$$H_2O + Kfs + Grt = Bt + Sil + Qtz \tag{3}$$

$$H_2O + Kfs + Sil = Ms + Qtz \tag{4}$$

$$Bt + Sil + Qtz = Grt + Ms. \tag{5}$$

Reaction (5) would decrease the $X_{Fe}$ of garnet, which conflicts with our chemical data. Thus, we favour a disequilibrium evolution, in which the reactants persisted out of their *P–T–X* stability field until reaction to the stable product assemblage was catalysed by deformation.

### Thermobarometry

Based on the mineral assemblage stable in ultramylonites and pre-mylonitic metapelites, the garnet–biotite exchange thermometer and the garnet–$Al_2SiO_5$–quartz–plagioclase (GASP) net-transfer barometer were used to evaluate the metamorphic conditions. In the mylonites, the Ferry & Spear (1978) calibration gave 510–570 °C for sample MM29 and 510–580 °C for sample MM30. The temperatures provided by the precursor metapelites are 590–690 °C. The estimated temperatures are largely dependent on the $X_{Fe}$ of garnet and are derived using the minima and maxima obtained for this parameter. Temperature estimates for the mylonitic stage are consistently higher than 500 °C, which is the minimum temperature for the stability of sillimanite (Holdaway, 1971).

Given the above temperature ranges, pressures estimated with the GASP barometer lie in the interval 0.1–0.35 GPa for the mylonitic stage. Only two calibrations (Hodges & Crowley, 1985; Koziol, 1989) provide pressures within the stability field of sillimanite at the calculated temperatures; the others are consistent with the presence of andalusite. Because sillimanite is inferred to have been stable in the ultramylonites, and because of the uncertainty of pressure values (±0.1 GPa), the resulting *P–T* conditions of equilibration during mylonite development are represented by the field B in Fig. 6. Because there are no variations in the Ca content of garnet and plagioclase during deformation, pressure values for the pre-mylonitic assemblage must lie along the same $K_{eq}$ line determined for the mylonitic conditions, and result in the field A in Fig. 6.

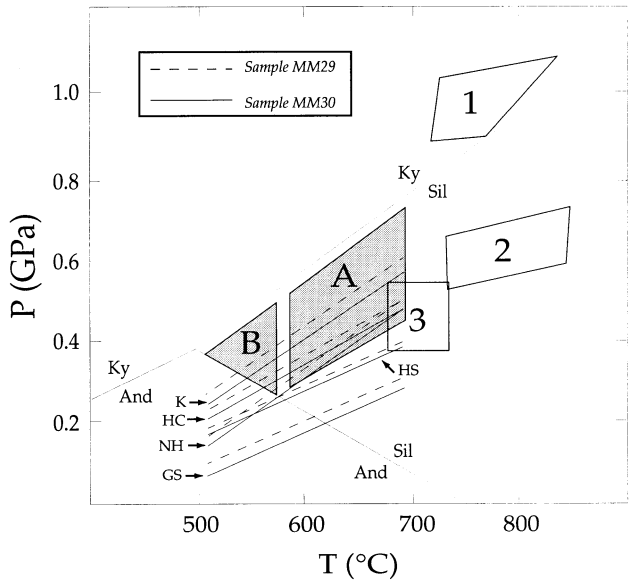


**Fig. 6.** Pre-Alpine *P–T* conditions for the Austroalpine Dent Blanche-Mont Mary system: fields A and B are the estimated conditions for high grade protolith and mylonites, respectively (this study); fields 1–3 refer to conditions estimated for the pre-Alpine metamorphism by Gardien *et al.* (1994) in the Dent Blanche nappe. GASP $K_{eq}$ lines: GS = Ganguly & Saxena (1984), HC = Hodges & Crowley (1985), HS = Hodges & Spear (1982), K = Koziol (1989), NH = Newton & Haselton (1981). Fields A and B are constrained on the basis of calculated garnet-biotite temperatures, sillimanite stability after Holdaway (1971), and $\pm 0.1$ GPa pressure error.

The syn-kinematic *P–T* conditions estimated in the studied mylonites point to a pre-Alpine age of deformation, because amphibolite facies metamorphic conditions were never reached during the Alpine orogeny in the Western Alps (Frey *et al.*, 1974; Niggli, 1978). Compared with the pre-Alpine *P–T* path reconstructed in the Valpelline metapelites of the Dent Blanche nappe by Gardien *et al.* (1994) (fields 1–3 in Fig. 6), the mylonites of the Mont Mary appear to record the latest metamorphic stage of the pre-Alpine history probably related to extensional tectonics.

## DISCUSSION

### Rheological conditions during deformation

The shape of the strength envelope for steady-state high-temperature creep (Ranalli & Murphy, 1987) indicates that rocks deforming in the ductile field support low differential stress at high homologous temperatures, whereas higher flow stresses are expected close to the brittle-ductile transition. The grain-size of dynamically recrystallized quartz, produced during steady-state creep, is related to the differential stress at the time of deformation and can be used as a piezometer (Mercier *et al.*, 1977; Twiss, 1977; Ord & Christie, 1984; and refs therein). A survey of literature data indicates a progressive grain-size reduction from regional tectonite foliations to discrete shear zones; this is consistent with progressive localization of deformation from the high to the low temperature ductile regime (Bak *et al.*, 1975; Smithson *et al.*, 1986). Moreover, it has been shown (e.g. Passchier, 1985; Etheridge & Wilkie, 1981) that the finest grain-size, in the range of several to a few tens of microns, is related to mylonites associated spatially with brittle structures, and such grain-sizes can thus be taken as the microstructure equilibrated at the highest differential stress supported during ductile flow close to the brittle-ductile transition. Therefore, in the pre-Alpine mylonites of Mont Mary nappe, the extremely fine grain-size of recrystallized quartz, in the range of the smallest values reported in the literature, points to deformation close to the brittle-ductile transition. This fact is also supported by the presence of ductilely deformed pseudotachylites in the mylonites, which has been regarded by several authors (e.g. Macaudiere & Brown, 1982; Passchier, 1982, 1985) as indicative of rheological conditions at the brittle-ductile transition. The syn–mylonitic origin for the Mont Mary nappe pseudotachylites is inferred from the persistence in deformed pseudotachylites of syn–kinematic amphibolite facies assemblages at the time of their ductile deformation, and by the absence of retrogradation in the mylonites during the fabric reactivation accompaning the pseudotachylite deformation. The Alpine greenschist facies assemblage is poorly developed and is post-kinematic to the foliation of pseudotachylites and mylonites. A deep seated generation of pseudotachylites may also explain the complete recrystallization of their groundmass and the absence of glass (Allen, 1979; Magloughlin & Spray, 1992). An alternative interpretation for ductilely deformed pseudotachylites was given by Hobbs *et al.* (1986), who suggested that pseudotachylites can be generated as ductile instabilities within the ductile regime, if below a critical temperature. Nonetheless, the temperature-strength field for unstable ductile flow occupies the high differential stress-low temperature region of the ductile field. Ductilely deformed pseudotachylites have also been attributed to the effect of resisters within the forming mylonites that act as stress risers: at a critical point the resisters fail, inducing a sudden increase of the strain rate and pseudotachylite formation (Koch & Mash, 1992). However, there is no systematic association of the Mont Mary nappe pseudotachylites with pods of relatively hard rocks (e.g. amphibolites) in mylonites; moreover, the pseudotachylites are confined to mylonites and do not involve the surrounding rocks.

The temperatures estimated for the pre-Alpine mylonitization are rather high to be at the level of the brittle-ductile transition in metapelites, because these rocks commonly undergo ductile flow even at lower greenschist facies conditions. In fact, the Alpine greenschist facies mylonites, developed from high-grade metapelites in the Austroalpine nappe of the

Western Alps, formed at lower temperatures (350–450 °C: Lattard, 1974; Mazurek, 1986; Pognante *et al*., 1987; Stunitz, 1989; Gardien *et al*., 1994) than the studied mylonites (510–580 °C). Therefore, contrasting rheological behaviour is envisaged in the metapelites during pre-Alpine and Alpine deformation, which implies migration of the brittle-ductile transition towards lower temperatures during the Alpine overprint. This rheological contrast may be explained by a different availability of aqueous fluids during the pre-Alpine and Alpine deformation, as well as by differences in strain rates.

#### Fluid behaviour

Any fluid model for the pre-Alpine mylonites of Mont Mary must fit the following observations:

(i) The presence of $H_2O$-bearing fluids during syn–mylonitic crystallization is required because reaction (1) involves hydration. No primary fluid inclusions were found, but the fluid composition may be inferred from mineral equilibria, using the stable mineral assemblage. Given the presence of graphite in the matrix, the fluid equilibrated with the mylonitic assemblage was a graphite-saturated COH fluid. The maximum mole fraction of $H_2O$ ($X_{H2O}$) in the fluid is constrained by the *P–T* conditions of metamorphism and, based on the calculations of Connolly & Cesare (1993), is 0.90–0.95. The minimum $X_{H2O}$ is defined by the stability of the assemblage Ms–Qtz–Sil: extrapolation of the data of Kerrick (1972) at the minimum calculated temperaure of 510 °C provides a lower limit of $X_{H_2O} = 0.3$.

(ii) Enough $H_2O$ must have been present to account for the significant decrease in bulk garnet amount (e.g. 0.5 wt% $H_2O$ for 10 wt% garnet consumed).

(iii) Dissolution-precipitation was active in the consumption of garnet edges associated with formation of biotite-rich pressure shadows. The effectiveness of these mechanisms implies the presence of an intergranular aqueous fluid.

(iv) On the other hand, the above mentioned high-temperature mylonite–pseudotachylite association and high strength conditions are consistent with water-deficient conditions. Similar mylonite–pseudotachylite associations have been interpreted in terms of water-deficient conditions in $CO_2$-dominated fluid systems (Passchier, 1985), and high-temperature generation of pseudotachylites has been reported in fluid-absent granulite facies rocks (Clarke & Norman, 1993). These features might also be explained in terms of high syn–mylonitic strain rates, but the absence, in pure quartz layers, of grain growth and annealing texture after the mylonitic stage are a strong argument in favour of water-deficient conditions. In fact, because pre-Alpine mylonites also experienced the Alpine metamorphic cycle, during which Alpine mylonites suffered extensive post-kinematic annealing, the absence of grain growth can only be related to the sluggish kinetics of coarsening under fluid-absent conditions (e.g. Rubie, 1986).

Provided the system remains closed to fluid infiltration, the above data, as a whole, can be explained in terms of transient water presence, determined by the progress of $H_2O$-consuming reactions such as (1). During the early stages of mylonitization, $H_2O$ is dominant in the fluid and assists plastic flow and mineral reactions; as reactions proceed, the amount of $H_2O$ is progressively decreased or eventually exhausted, so that the final stages of mylonitization occur under water-deficient conditions.

#### Deformation-induced water-deficient conditions

We have suggested above that the syn–kinematic occurrence of $H_2O$-consuming reactions may cause the progressive development of water-deficient conditions in mylonites by reducing the amount of free $H_2O$. It is now suggested that, in a closed system, the syn–mylonitic grain-size reduction may also induce the water-deficient character and prevent further ductile deformation and grain growth.

Grain-size reduction is often regarded as a main softening mechanism in mylonites (White *et al*., 1980) and this is commonly supported by localization of deformation in fine-grained rocks. Strain softening is commonly related to a change in deformation mechanism from intracrystalline plasticity to a mechanism in which grain boundary sliding dominates (e.g. Fitz Gerald & Stunitz, 1993). However, the latter process is able to produce a marked softening in the presence of intergranular free $H_2O$, while fluid-absent, fine-grained aggregates may be relatively hard to deform (Pennacchioni, 1996). In fact the process of grain boundary sliding needs some accommodating mechanism such as diffusive and/or plastic mass transfer (e.g. Gifkins, 1976; McClay, 1977), and both mechanism are strongly enhanced by the presence of a free aqueous fluid (e.g. Tullis & Yund, 1989; Rutter, 1972; Faver & Yund, 1992). Because the rate of the accommodating mechanism controls the rate of the bulk flow, the softening effect during grain-size reduction is strongly dependent on the presence of a free aqueous fluid.

Rubie (1986) suggested that intergranular diffusion coefficients approach the values of lattice diffusion coefficients when the intergranular fluid film becomes thinner than a double molecular layer ($\cong 50$ nm). The strong effect of the wetting characteristics of an aggregate on the diffusion rates has also been documented experimentally (Farver & Yund, 1992; Tullis *et al*., 1996). Because grain-size reduction is accompanied by an increase of the grain boundary area, it must strongly reduce the thickness of the fluid film in a closed system.

The effect of grain-size reduction on fluid film thickness is schematized in the following model that assumes: (i) closed system; (ii) cubic shape of mineral grains, (iii) 0.1 Vol. % free $H_2O$, and (iv) complete,

homogeneous grain boundary wetting by fluid film. Such a fluid film distribution is supported by experimental investigations (Urai, 1983; Jin *et al*., 1994; Tullis *et al*., 1996) which demonstrate that under differential stress a complete grain boundary wetting may be achieved. With these assumptions, if the initial grain-size of the rock is 1 mm (same order of grain-size of the undeformed studied metapelites) the corresponding fluid film thickness is 0.33 $\mu$m. During mylonitization the grain-size reduction decreases the thickness of the grain boundary fluid film: with a grain-size of 0.1 mm, the fluid film thins to 0.03 μm. In this situation, a free water fluid film is still present and the grain-size reduction results in a strain softening, allowing viscous grain boundary sliding assisted by diffusion.

When the average grain-size is reduced to 1 $\mu$m (similar to the grain-size of the studied ultramylonite), the same amount of fluid forms a continuous film of 33 nm, thinner than the minimum predicted for a 'bulk fluid' (Rubie, 1986). This situation corresponds to a water-deficient condition and the resulting effect is strain hardening.

The example above is qualitative, but demonstrates that the thickness of a fluid film decreases linearly with grain-size. The same conclusion also holds for other types of fluid distribution (e.g. tubules or cavities). As a consequence, the ability of a fluid to wet grain boundaries is directly proportional to grain-size: when a critical value is reached, all water can be structurally incorporated within the disordered lattice of grain boundaries, so that a free aqueous phase is no longer present. Provided a system is closed to $H_2O$, extreme grain-size reduction during mylonitization may result in evolution to water-deficient conditions, even without the occurrence of a concurrent $H_2O$-consuming reaction. Thus, *even in a fluid-present situation*, a substantial decrease of fluid availability and activity is to be expected in part or all of the micron-sized matrix of the ultramylonites, resulting in very low diffusion coefficients that are likely to inhibit both diffusion creep and grain-size coarsening.

Note that this scenario is somewhat different to that of the 'water-deficient' mylonites described by Passchier (1985) and related to a low $H_2O$ fraction in a $CO_2$-rich metamorphic fluid. In the case where there is extreme grain-size reduction, decreased $H_2O$ activity and availability are also to be expected in the case of a pure $H_2O$ fluid.

To summarise, the softening effect of grain-size refinement may be reduced or even completely lost where $H_2O$ availability is low. In the pre-Alpine ultramylonites grain-size reduction is accompanied by, and possibly enhances, a progressive decrease in free water and the end case may be that of strain hardening. This may explain how such extremely fine-grained rocks may undergo brittle instabilities. From the rheological point of view, the rock-strength envelope gradually migrates, during deformation, towards higher temperatures with the consequent increment in the strength level and development of transient brittle instabilities close to the brittle-ductile transition. The coexistence of plastic flow and brittle instabilities (pseudotachylites) in adjacent domains of mylonites may also be interpreted in terms of spatially heterogeneous fluid distribution owing to low rock permeability.

## CONCLUSIONS

Some mylonites in the Mont Mary nappe developed under amphibolite facies conditions at 510–580 °C and 0.25–0.45 GPa. They are part of the latest phase of the pre-Alpine metamorphic path related to an extensional regime.

The rheological conditions of deformation are estimated to be close to the brittle-ductile transition from the high differential stress and the occurrence of ductilely deformed pseudotachylites. This would require water-deficient conditions at the estimated temperature that is in accord with the absence of significant grain growth of quartz aggregates during the post-mylonitic thermal history. However, the development of the syn–kinematic assemblage requires the presence of $H_2O$ according to the calculated mass balance reaction.

This apparent inconsistency can be explained in terms of progressive water depletion in a closed system, that is accomplished through the progress of $H_2O$-consuming reactions. The grain-size reduction by dynamic recrystallization, which inhibits the connectivity of the intergranular fluid, is an additional potential mechanism for decreasing $H_2O$ availability.

During the Alpine overprint the re-establishment of ductile deformation required the introduction of an aqueous fluid in the high-grade metapelites. The limited and localized development of Alpine mylonites may be related to the low water availability at the nappe scale, inhibiting pervasive ductile deformation and, consequently, metamorphic re-equilibration. In this view, the Mont Mary provides a straightforward example of the control of fluids on the rheological properties and kinetic behaviour of metapelitic rocks.

## ACKNOWLEDGEMENTS

Financial support from CNR (Centro di Studio per la Geodinamica Alpina) and M.U.R.S.T. 40% and 60% (P. F. Sassi & G. V. Dal Piaz). We thank T. Andersen, G. L. Fruh-Green, J. Tullis and R. Vernon for reviews, and G.V. Dal Piaz, P. F. Sassi and R. Spiess for reading and improving the early versions of the manuscript. The help of C. Brogiato and S. Castelli (photography), G. Giorgetti (AEM), P. Guerriero and S. Zandolin (SEM), and A. Novello (thin sections) was also greatly appreciated.

## REFERENCES


Allen, A. R., 1979. Mechanism of frictional fusion in fault zones. *Journal of Structural Geology*, **1,** 231–243.

Andersen, T., Austrheim, H. & Burke, E. A. J., 1991. Fluid-induced retrogression of granulites in the Bergen Arcs, Caledonides of W. Norway: Fluid inclusion evidence from amphibolite-facies shear zones. *Lithos*, **27,** 29–42.

Bak, J., Grocott, J., Korstgard, J. A., Sorenson, K., Nash, D. F. & Watterson, J., 1975. Tectonic implications of Precambrian shear belts in western Greenland. *Nature*, **254,** 566–569.

Ballevre, M., Kienast, J. -R. & Vuichard, J. -P., 1986. La 'nappe de la Dent-Blanche' (Alpes occidentales): Deux unites austroalpines independantes. *Eclogae geologicae Helveticae*, **79,** 57–74.

Boundy, T. M., Fountain, D. M. & Austrheim, H., 1992. Structural development and petrofabric of eclogite facies shear zones, Bergen Arcs, western Norway: implications for deep crustal deformation processes. *Journal of Metamorphic Geology*, **10,** 127–146.

Burkhard, M. & Kerrig, R., 1988. Fluid regimes in the deformation of the Helvetic nappes, Switzerland, as inferred from stable isotope data. *Contributions to Mineralogy and Petrology*, **99,** 416–429.

Canepa, M., Castelletto, M., Cesare, B., Martin, S. & Zaggia, L., 1990. The Austroalpine Mont Mary Nappe (Italian Western Alps). *Memorie di Scienze Geologiche*, **42,** 1–17.

Christie, J. M. & Ord, A., 1980. Flow stress from microstructures of mylonites: example and current assessment. *Journal of Geophysical Research*, **85,** 6253–6262.

Clarke, G. L. & Norman, A. R., 1993. Generation of pseudotachylite under granulite facies conditions, and its preservation during cooling. *Journal of Metamorphic Geology*, **11,** 319–335.

Connolly, J. & Cesare, B., 1993. C-O-H-S fluid composition and oxygen fugacity in graphitic metapelites. *Journal of Metamorphic Geology*, **11,** 379–388.

Dal Piaz, G. V., 1993. Evolution of the Austro-Alpine and Upper Penninic Basement in the Northwestern Alps from Variscan Convergence to Post-Variscan Extension. In: *Pre-Mesozoic Geology in the Alps* (eds von Raumer, J. F. & Neubauer, F.), pp. 327–344. Springer-Verlag, Amsterdam.

De Leo, S., Biino, G. & Compagnoni, R., 1987. Riequilibrazioni metamorfiche Alpine nella serie di Valpelline e di Arolla a Nord di Bionaz (Valpelline, Aosta). *Rendiconti della Societa Italiana di Mineralogia e Petrografia*, **42,** 181–182.

Diehl, E. A., Masson, R. & Stutz, A. H., 1952. Contributi alla conoscenza del ricoprimento Dent Blanche. *Memorie dell'Istituto di Geologia e Mineralogia dell'Universita di Padova*, **17,** 1–53.

Etheridge, M. A. & Wilkie, J. C., 1981. An assessment of dynamically recrystallized grain-size as a palaeopiezometer in quartz-bearing mylonite zones. *Tectonophysics*, **78,** 475–508.

Farver, J. R. & Yund, R. A., 1992. Oxygen diffusion in a fine-grained quartz aggregate with wetted and nonwetted microstructures. *Journal of Geophysical Research*, **97,** 14017–14029.

Ferry, J. M. & Spear, F. S., 1978. Experimental calibration of the partitioning of Fe and Mg between biotite and garnet. *Contributions to Mineralogy and Petrology*, **66,** 113–117.

Fisher, G. W., 1989. Matrix analysis of metamorphic mineral assemblages and reactions. *Contributions to Mineralogy and Petrology*, **102,** 69–77.

Fitz Gerald, J. D. & Stunitz, H., 1993. Deformation of granitoids at low metamorphic grade. I: Reactions and grain size reduction. *Tectonophysics*, **221,** 269–297.

Frey, M., Hunziker, J. C., Frank, W., Bocquet, J., Dal Piaz, G. V., Jaeger, E. & Niggli, E., 1974. Alpine metamorphism of the Alps: a review. *Schweizerische mineralogische und petrographische Mitteilungen*, **54,** 247–290.

Fruh-Green, G. L., 1994. Interdependence of deformation, fluid infiltration and reaction progress recorded in eclogitic metagranitoids (Sesia Zone, Western Alps). *Journal of Metamorphic Geology*, **12,** 327–343.

Ganguly, J. & Saxena, S. K., 1984. Mixing properties of aluminosilicate garnets: constraints from natural and experimental data, and applications to geothermo-barometry. *American Mineralogist*, **69,** 88–97.

Gardien, V., Reusser, E. & Marquer, D., 1994. Pre-Alpine metamorphic evolution of the gneisses from the Valpelline serie (Western Alps, Italy). *Schweizerische mineralogische und petrographische Mitteilungen*, **74,** 489–502.

Gardien, V., Reusser, E. & Marquer, D., 1995. Compared P-T evolutions between a paleo (Valpelline Series) and an actual (Galicia, Spain) continental margins. *Terra Abstracts*, **7,** 125.

Gibson, R. G., 1990. Nucleation and growth of retrograde shear zones: an example from the Needle Mountains, Colorado, U.S.A. *Journal of Structural Geology*, **12,** 339–350.

Gifkins, R. C., 1976. Grain boundary sliding and its accommodation during creep and superplasticity. *Metallurgical Transactions*, **7,** 1225–1232.

Grocott, J., 1981. Fracture geometry of pseudotachylyte generation zones: a study of shear fractures formed during seismic events. *Journal of Structural Geology*, **3,** 169–178.

Guidotti, C. V., 1984. Micas in metamorphic rocks. *Reviews in Mineralogy*, **13,** 357–468.

Hanmer, S., 1986. Asymmetrical pull-aparts and foliation fish as kinematic indicators. *Journal of Structural Geology*, **8,** 111–122.

Hirth, G. & Tullis, J., 1992. Dislocation creep regimes in quartz aggregates. *Journal of Structural Geology*, **14,** 145–159.

Hobbs, B. E., Means, W. D. & Williams, P. F., 1976. An Outline of Structural Geology, pp. 571. John Wiley, New York.

Hobbs, B. E., Ord, A. & Teyssier, C., 1986. Earthquakes in the ductile regime? *Pure and Applied Geophysics*, **124,** 309–336.

Hodges, K. V. & Crowley, P. D., 1985. Error estimation and empirical geothermobarometry for pelitic systems. *American Mineralogist*, **70,** 702–709.

Hodges, K. V. & Spear, F. S., 1982. Geothermometry, geobarometry and the $Al_2SiO_5$ triple point at Mt. Moosilauke, New Hampshire. *American Mineralogist*, **67,** 1118–1134.

Holdaway, M. J., 1971. Stability of andalusite and the aluminum silicate phase diagram. *American Journal of Science*, **271,** 97–131.

Jin, Z. -M., Green, H. W. & Zhou, Y., 1994. Melt topology during dynamic partial melting of peridotite. *Nature*, **372,** 164–167.

Kerrich, R., 1986. Fluid infiltration into fault zones: chemical, isotopic, and mechanical effects. *Pure and Applied Geophysics*, **124,** 225–268.

Kerrick, D. M., 1972. Experimental determination of muscovite + quartz stability with $P_{H2O} < P_{total}$. *American Journal of Science*, **272,** 946–958.

Kerrich, R., 1986. Fluid infiltration into fault zones: chemical, isotopic, and mechanical effects. *Pure and Applied Geophysics*, **124,** 225–268.

Kerrick, D. M., 1972. Experimental determination of muscovite + quartz stability with $P_{H2O} < P_{total}$. *American Journal of Science*, **272,** 946–958.

Koch, N. & Masch, L., 1992. Formation of Alpine mylonites and pseudotachylytes at the base of the Silvretta nappe, Eastern Alps. *Tectonophysics*, **204,** 289–306.

Koziol, A. M., 1989. Recalibration of the garnet-plagioclase-$Al_2SiO_5$-quartz (GASP) geobarometer and application to natural parageneses. *EOS, Transactions American Geophysical Union*, **70,** 493.

Kronenberg, A. K., Segall, P. & Wolf, G. H., 1990. Hydrolytic weakening and penetrative deformation within a natural shear zone. *American Geophysical Union Monographic Series*, **56,** 21–36.

Lardeaux, J. M. & Spalla, M. I., 1991. From granulites to eclogites in the Sesia zone (Italian Western Alps): a record of the opening and closure of the Piedmont ocean. *Journal of Metamorphic Geology*, **9,** 35–59.

Lattard, D., 1974. *Les roches du facies schist vert dans la zone du Sesia-Lanzo*. These 3eme Cycle, Paris, 76 pp.

Macaudiere, J. & Brown, W. L., 1982. Transcrystalline shear fracturing and pseudotachylite generation in a meta-anorthosite (Harris, Scotland). *Journal of Structural Geology*, **4,** 395–406.

Magloughlin, J. F. & Spray, J. G., 1992. Frictional melting processes and products in geological materials: introduction and discussion. *Tectonophysics*, **204,** 197–206.

Masson, R., 1938. Geologisch-Petrographische Untersuchungen im unteren Valpelline, Provinz Aosta (Italien). *Schweizerische mineralogische und petrographische Mitteilungen*, **18,** 54–213.

Mazurek, M., 1986. Structural evolution and metamorphism of the Dent Blanche nappe and Combin zone west of Zermatt (Switzerland). *Eclogae Geologicae Helveticae*, **79,** 41–56.

McCaig, A. M., 1988. Deep circulation in fault zones. *Geology*, **16,** 867–870.

McClay, K. R., 1977. Pressure solution and Coble creep in rocks and minerals: a review. *Journal of the Geological Society of London*, **134,** 57–70.

Mercier, J. -C., Anderson, D. A. & Carter, N. L., 1977. Stress in the lithosphere: Inferences from steady-state flow of rocks. *Pure and Applied Geophysics*, **115,** 199–226.

Newton, R. C. & Haselton, H. T., 1981. Thermodynamics of the garnet-plagioclase-$Al_2SiO_5$-quartz geobarometer. In: *Thermodynamics of Minerals and Melts* (ed. Newton, R. C.). *Advances in Physical Geochemistry*, **1,** 131–148.

Nicot, E., 1977. *Les roches meso et catazonales de la Valpelline (nappe Ide la Dent Blanche; Alpes italiennes)*. These 3eme Cycle, Paris, 211 pp.

Niggli, E., 1978. Metamorphic map of the Alps, 1: 1.000.000 and explanatory text. *Subcommission for the Cartography of the Metamorphic Belts of the World, Leiden and Unesco, Paris.*

Ord, A. & Christie, J. M., 1984. Flow stresses from microstructures in mylonitic quartzites of the Moine Thrust zone, Assynt area, Scotland. *Journal of Structural Geology*, **6,** 639–654.

Passchier, C. W., 1985. Water-deficient mylonite zones – An example from the Pyrenees. *Lithos*, **18,** 115–127.

Passchier, C. W. & Simpson, C., 1986. Porphyroclast systems as kinematic indicators. *Journal of Structural Geology*, **8,** 831–843.

Peacor, D. R., 1992. Analytical electron microscopy: X-ray analysis. In: *Minerals and Reactions at the Atomic Scale: Transmission Electron Microscopy* (ed. Buseck, P. R.). *Reviews in Mineralogy*, **27,** 113–140.

Pennacchioni, G., 1996. Progressive eclogitization under fluid-present conditions of pre-Alpine mafic granulites in the Austroalpine Mt Emilius Klippe (Italian Western Alps). *Journal of Structural Geology*, **18,** 549–561.

Pennacchioni, G. & Guermani, A., 1993. The mylonites of the Austroalpine Dent Blanche nappe along the northwestern side of the Valpelline Valley (Italian Western Alps). *Memorie di Scienze Geologiche*, **45,** 37–55.

Pognante, U., Talarico, F., Rastelli, N. & Ferrati, N., 1987. High pressure metamorphism in the nappes of the Valle dell'Orco traverse (Western Alps collisional belt). *Journal of Metamorphic Geology*, **5,** 397–414.

Polino, R., Dal Piaz, G. V. & Gosso, G., 1990. Tectonic erosion at the Adria margin and accretionary processes for the Cretaceous orogeny in the Alps. *Memoires de la Societe geologique de France*, **156,** 345–367.

Ranalli, G. & Murphy, D. C., 1987. Rheological stratification of the lithosphere. *Tectonophysics*, **132,** 281–295.

Rubie, D. C., 1986. The catalysis of mineral reactions by water and restrictions on the presence of aqueous fluid during metamorphism. *Mineralogical Magazine*, **50,** 399–415.

Rutter, E. H., 1972. The influence of interstitial water on the rheological behaviour of calcite rocks. *Tectonophysics*, **14,** 13–33.

Segall, P. & Simpson, C., 1986. Nucleation of ductile shear zones on dilatant fractures. *Geology*, **14,** 56–59.

Sibson, R. H., 1975. Generation of pseudotachylyte by ancient seismic faulting. *Geophysical Journal of the Royal Astronomic Society*, **43,** 775–794.

Smith, C. S. & Guttman, L., 1953. Measurement of internal boundaries in three-dimensional structures by random sectioning. *Transactions of the American Institute of Mining and Metallurgical Engineers*, **197,** 81–87.

Smithson, S. B., Johnson, R. A. & Hurich, C. A., 1986. Crustal reflections and crustal structure. In: *Reflection Seismology: The Continental Crust* (eds Barazangi, M. & Brown, L.). *American Geophysical Union, Geodynamic Serie*, **14,** 21–32.

Stunitz, H., 1989. Partitioning of metamorphism and deformation in the boundary region of the 'Seconda Zona Diorito-Kinzigitica', Sesia Zone, Western Alps. *PhD thesis, University of Zurich, Zurich*, 255 pp.

Stutz, A. H. & Masson, R., 1938. Zur Tektonik der Dent Blanche Decke. *Schweizerische mineralogische und petrographische Mitteilungen*, **18,** 40–53.

Swanson, M. T., 1992. Fault structure, wear mechanisms and rupture processes in pseudotchylyte generation. *Tectonophysics*, **204,** 223–242.

Tobisch, O. T., Barton, M. D., Vernon, R. H. & Paterson, S. R., 1991. Fluid-enhanced deformation: transformation of granitoids to banded mylonites, western Sierra Nevada, California, and southeastern Australia. *Journal of Structural Geology*, **13,** 1137–1156.

Tullis, J. & Yund, R. A., 1989. Hydrolytic weakening of quartz aggregates: The effects of water and pressure on recovery. *Geophysical Research Letters*, **16,** 1343–1346.

Tullis, J., Yund, R. & Farver, J., 1996. Deformation-enhanced fluid distribution in feldspar aggregates and implications for ductile shear zones. *Geology*, **24,** 63–66.

Twiss, R. J., 1977. Theory and applicability of a recrystallized grain size paleopiezometer. *Pure and Applied Geophysics*, **115,** 227–244.

Urai, J. L., 1983. Water assisted dynamic recrystallization and weakening in polycrystalline bischoffite. *Tectonophysics*, **96,** 125–157.